X-ray absorption spectroscopy of strongly disordered glasses: Local structure around Ag ions in g-Ag$_2$O$\cdot n$B$_2$O$_3$

A. Kuzmin*

Institute of Solid State Physics, University of Latvia, Kengaraga Street 8, LV-1063 Riga, Latvia

G. Dalba and P. Fornasini

Istituto Nazionale per la Fisica della Materia and Dipartimento di Fisica, Università di Trento, Via Sommarive 14, I-38050 Povo (Trento), Italy

F. Rocca

IFN-CNR, Istituto di Fotonica e Nanotecnologie del Consiglio Nazionale delle Ricerche, Sezione "ITC-CeFSA" di Trento, Via Sommarive 18, I-38050 Povo (Trento), Italy

O. Šipr

Institute of Physics, Academy of Sciences of the Czech Republic, Cukrovarnická 10, CZ-162 53 Prague, Czech Republic

The local structure around Ag ions in silver borate glasses g-Ag$_2$O$\cdot n$B$_2$O$_3$ ($n = 2, 4$) was studied by x-ray absorption spectroscopy at the Ag K edge for temperatures from 77 to 450 K. Extended x-ray absorption fine structure (EXAFS) analysis based on cumulant expansion or multishell Gaussian model fails for these systems. Therefore, the radial distribution functions (RDFs) around Ag ions were reconstructed using a method based on the direct inversion of the EXAFS expression. The RDFs consist of about eight atoms (oxygens and borons), exhibit a relatively weak temperature dependence, and indicate the presence of strong static disorder. Two main components can be identified in RDFs, located at about 2.3–2.4 Å and 2.5–3.4 Å, respectively. The chemical types of atoms contributing to the RDF were determined via a simulation of configurationally averaged x-ray absorption near-edge structure (XANES) and EXAFS signals. The immediate neighborhood of Ag contains mostly oxygens while borons dominate at larger distances. The combination of EXAFS and XANES techniques allowed us to determine a more complete structural model than would be possible by relying solely on either EXAFS or XANES alone.

PACS number(s): 61.43.Fs, 61.10.Ht, 78.70.Dm

I. INTRODUCTION

Silver borate glasses g-Ag$_2$O$\cdot n$B$_2$O$_3$ stimulate a considerable interest as fast-ion conductors, especially when doped with AgI.[1,2] They can be produced in a wide range of compositions, allowing for a continuous change of their physical properties. Borate glasses are network glasses based on trigonal BO$_3$ and tetrahedral BO$_4$ units organized in more complex superstructural elements. Depending on the amount of the modifier oxide (in our case Ag$_2$O), the relative concentration of threefold- and fourfold-coordinated boron varies, and consequently the distribution of negative charges available for the bonding of silver cations changes as well. Because of the high mobility of Ag ions and the multiplicity of sites available for the bonding with the borate network, a deep knowledge of the local structure around Ag ions is still an open problem—despite the fact that the structure of silver borate glasses was studied by x-ray and neutron scattering[3–11] and by x-ray absorption spectroscopy[12–18] for years. The purpose of this paper is to obtain more refined information on the local environment of Ag ions by investigating the x-ray absorption fine structure (XAFS) via a refined joint analysis of both x-ray absorption near-edge structure (XANES) and extended x-ray absorption fine structure (EXAFS).

XAFS is a powerful tool to study the local atomic and electronic structure in disordered materials.[19] It offers a local view on the system geometry from a particular chemically specific site. Therefore, it provides a site-selective radial distribution function (RDF), centered at atoms of only one chemical type. The theory of XAFS has been significantly improved during the last ten years[20] and allows nowadays a rather accurate description of x-ray absorption fine structure for frozen atomic configurations.[21–25] It is in fact possible to use a single formalism for describing x-ray absorption in the XANES and EXAFS regions.[20] However, for practical purposes it is useful to maintain the distinction between XANES and EXAFS. One reason is that a full multiple scattering should be normally used in the XANES region (for photoelectron energies up to 50–70 eV above the absorption edge), whereas a truncated multiple-scattering series can be utilized at higher energies. The degree of approximation introduced by the truncated multiple-scattering series strongly depends on the local structure and chemical composition of a particular compound. In many practical cases, the single-scattering term is dominant.[19] Another reason for analyzing XANES and EXAFS separately is that a different level of agreement between theory and experiment can be achieved in the two regions. Calculated and measured EXAFS oscillations agree quite well in typical situations.[19,20] On the other

hand, current XANES calculations usually do not reproduce the measured spectrum with such an accuracy (mainly because of non-muffin-tin and many-body effects, which are difficult to account for and are more important for low photoelectron energies). At the same time, multiple scattering of the photoelectron and energy dependence of its scattering by various atoms may cause that some aspects of the local structure are better observable through XANES than through EXAFS. Therefore, a separate analysis of XANES and EXAFS could be advantageous in many cases.

In spite of the progress in the XAFS theory, the evaluation of static and dynamic disorder is still a weak point. In the EXAFS region, the disorder is usually taken into account by describing each scattering path through a distribution of interatomic distances. Single scattering paths, corresponding to *identified* coordination shells, are often singled out by Fourier filtering. When dealing with moderately disordered systems, the distributions of distances can be parametrized in terms of a few leading cumulants.[26,27] Although in the case of purely thermal disorder the effectiveness of the procedure of Fourier filtering plus cumulant analysis can be checked by means of accurate temperature-dependent measurements,[28] in case of structural disorder no simple self-consistency criteria can be adopted, and the reliability of structural information can be, in some cases, highly questionable.

Early EXAFS studies of g-Ag$_2$O$\cdot n$B$_2$O$_3$ at the Ag K and L_3 edges, based on Fourier filtering and cumulant analysis limited to the harmonic terms, indicated that silver is coordinated by two oxygens (like in crystalline Ag$_2$O).[12–14] The Ag-O distances were evaluated as 2.2–2.3 Å (to be compared to 2.04 Å in c-Ag$_2$O). The low coordination number was supported by a qualitative comparison of the Ag L_3 edge structure in glasses and in c-Ag$_2$O.[12–14] However, this picture is somewhat different from results obtained in the last decade on the basis of scattering techniques.

X-ray and neutron scattering methods provide a total RDF when applied to noncrystalline systems. Such an RDF reflects mutual distances between all possible atomic pairs present in a solid and can be thus seen as a superposition of several "partial" or site-related RDFs. Based on best-fitting of experimental structure factors, the peaks in the total RDF are then attributed to contributions from particular atomic pairs. Procedures based on modeling the RDF by a set of Gaussians were used in Refs. 3–6, whereas a more sophisticated reverse Monte Carlo technique and an *ad hoc* cluster modeling were employed in Refs. 7–11. All scattering experiments agree that the total RDFs in silver borate glasses are characterized by two peaks at ~1.4 and 2.4 Å (both being better resolved in the neutron data than in the x-ray data). The first RDF peak corresponds to the shortest B-O distances, located at 1.37 Å for the BO$_3$ units and at 1.47 Å for the BO$_4$ units. The second peak in the total RDF is due to contributions from several different atomic pairs: Ag-O, O-O, and B-B bond lengths are evaluated to be about 2.4 Å, the second shell B-O distance about 2.8–2.9 Å, and the Ag-B distance about 3.1 Å. The overlap between these contributions, however, makes an accurate determination of interatomic distances difficult. Even more complicated is the quantification of the coordination number of Ag ions: 3.0–3.7 neighboring oxygen atoms were found by Swenson

et al.[5,9,11] contrary to about six atoms found by Ushida *et al.*[6] The existence of an Ag-Ag contribution, with average coordination number about 1.0 in tetraborate and about 2.0 in diborate glasses,[9,11] was also proposed at distances 3.0–4.5 Å.[5,8–11] In any case, scattering data indicate that Ag ions are surrounded by a much higher number of neighbors and within a larger range than what was suggested in earlier XAFS studies.

The apparent disagreement between results obtained by scattering and by EXAFS methods can be understood in the light of more recent XANES studies.[29,30] The calculated Ag K edge XANES of g-Ag$_2$O$\cdot n$B$_2$O$_3$ could be reconciled with experiments only if disorder is explicitly taken into account via the so-called multiconfiguration approach.[29] By analyzing the Ag K edge XANES, it was found that, on the average, Ag ions in silver borate glasses are coordinated by approximately four oxygens, with Ag-O distances between 2.0 and 2.4 Å, followed by approximately four borons located between 2.5 and 3.0 Å (Ref. 29). At the same time, it was found that the Ag K edge XANES in g-Ag$_2$O$\cdot n$B$_2$O$_3$ is not very sensitive to more finer details of the RDF; it is thus not possible to get more accurate results by analyzing XANES alone. For more complete information, it is necessary to use EXAFS data, which span a larger k-space interval and, thus, contain more structural information.

In view of this situation, we are now presenting a more complex approach, which combines both EXAFS and XANES analyses. EXAFS data at the Ag K edge are analyzed to obtain a radial distribution function without relying on the cumulant expansion method; successively, this RDF is used as structural constraint for a multiconfiguration XANES and EXAFS analysis. In this way, a more comprehensive view on the local structure around Ag ions can be obtained. The plan of the paper is the following. We start with introducing our experiment in Sec. II. Then methods of EXAFS and XANES analyses are discussed in Sec. III. After attempting to analyze EXAFS via cumulant expansion and multishell Gaussian model in Secs. IV A and IV B, we proceed by applying the hybrid regularization–least-squares-fitting approach to reconstruct the RDF in Sec. IV C. Our investigation is completed by analyzing the XANES data in Sec. IV D. Finally, the main results are discussed and summarized in Secs. V and VI.

II. EXPERIMENTAL DETAILS

The samples of binary silver borate glasses g-Ag$_2$O$\cdot n$B$_2$O$_3$ were prepared by a standard melt-quenching procedure.[31] The absence of any crystalline phase in the glasses was confirmed by x-ray scattering measurements. X-ray absorption spectra were measured at the Ag K edge using the synchrotron radiation from the ESRF storage ring (Grenoble, France) at the GILDA CRG BM08 beamline, operated in the high-energy configuration, without focusing. The transmission scheme with a Si(311) crystal monochromator and two ion chambers filled with argon gas was used. The experimental energy resolution was about 2.5 eV, which is well below the Ag $1s$ core hole lifetime. Spectra of the silver diborate glass g-Ag$_2$O$\cdot 2$B$_2$O$_3$ and of the silver tet-

raborate glass g-$Ag_2O \cdot 4B_2O_3$ were measured in the range of temperatures T from 77 to 450 K. The spectrum of crystalline c-Ag_2O, measured at 77 K, was used as a reference.

III. METHODS OF EXAFS AND XANES ANALYSIS

A. Extraction of EXAFS signal

The EXAFS signal $\chi(k)$ is conventionally defined as

$$\chi(k) = \frac{\mu_{exp}(E) - \mu_0(E) - \mu_b(E)}{\mu_0(E)}, \qquad (1)$$

where $\mu_{exp}(E)$ is the experimental absorption coefficient, $\mu_b(E)$ is the pre-edge background extrapolated beyond the absorption edge, $\mu_0(E)$ is the atomiclike contribution, and $k = [(2m_e/h^2)(E-E_0)]^{1/2}$ is the wave vector, with E_0 being the photoelectron energy origin. In the EDA package,[32] which we used for extracting the EXAFS oscillations, the $\mu_0(E)$ signal is written as $\mu_0(E) = \mu_0^I(E) + \mu_0^{II}(k) + \mu_0^{III}(k)$ and components $\mu_0^I(E)$, $\mu_0^{II}(k)$, and $\mu_0^{III}(k)$ are determined one by one using an original three-step procedure.[33] In the first step of this procedure, the component $\mu_0^I(E)$ is found in the E space as a polynomial of the n order ($0 \leq n \leq 10$). In the second step, another polynomial $\mu_0^{II}(k)$ is found in the k space. In the third step, the remaining $\mu_0^{III}(k)$ component is determined by smoothing cubic splines. The main idea of the three-step procedure is to find such $\mu_0(E)$ that minimizes the low-frequency nonstructural contribution to EXAFS while leaving the structural part undisturbed. This is achieved in the EDA package within an interactive procedure by a simultaneous control of the shape of the EXAFS signal in the k space and of its Fourier transform in the R space.[33] The experimental EXAFS signals for the reference compound c-Ag_2O and for borate glasses, extracted using the procedure described above, are shown in Figs. 1 and 2, respectively.

An important point of the EXAFS data analysis is the correct choice of E_0, since it influences the amplitude and the phase of the EXAFS signal (especially at low-k values). The accuracy with which interatomic distances can be determined is thereby restricted. In order to achieve the best results, the E_0 position should be set in the same way in the EXAFS signal to be analyzed and in the EXAFS signal of the reference compound that is used to determine the scattering amplitudes and phase shifts for the atomic pairs of interest. The reference EXAFS signal can be either obtained experimentally from a compound with a known atomic structure or calculated by one of the available *ab initio* codes.[21–23]

B. Reference EXAFS signals

In this work, the FEFF8 code[21] was used to generate the reference signal. For this purpose, we constructed a cluster of 8 Å radius with the structure of c-Ag_2O (lattice parameter $a=4.72$ Å),[34] containing 11 shells around Ag. In order to obtain the potential, a self-consistent calculation with a complex Hedin-Lundqvist exchange-correlation potential was performed for a smaller cluster of six shells. The muffin-tin radii were 1.390 Å for the central Ag atom (with a core hole in the $1s$ level), 0.972 Å for the O atoms, and 1.374 Å for
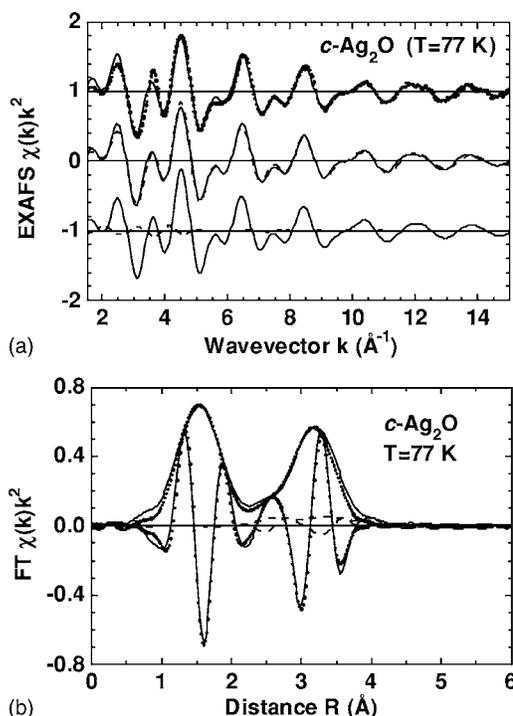
FIG. 1. Comparison of the experimental and best-fitted Ag K-edge EXAFS signals and their FTs in c-Ag_2O. Upper panel: the uppermost pair of curves shows a comparison of the full experimental signal (dotted line) with the experimental signal back-Fourier filtered in the R-space range from 0.5 to 4.0 Å and corresponding thus to the first three coordination shells (full line); the middle pair of curves shows the back-Fourier filtered experimental signal (full line) and the result of the best-fitting procedure (dashed line); the lowermost pair of curves shows the decomposition of the best-fitted signal into the sum of single-scattering contributions from the first three coordination shells (full line) and into a double-scattering Ag-O_1-Ag_2-Ag contribution (dashed line). Lower panel: the FTs of the experimental (dotted lines) and best-fitted (full lines) EXAFS signals, calculated in the k-space range 2.0–9.0 Å^{-1}. Both the modulus and imaginary parts of FTs are shown. The dashed line corresponds to the double-scattering Ag-O_1-Ag_2-Ag contribution.

the other Ag atoms. The EXAFS signal calculated in this way was used (i) to align the energy scale of the experiment with theory, thus eliminating the E_0 parameter from the fitting procedure, and (ii) to estimate the value of the amplitude scaling factor S_0^2, which was used later on in determining the coordination numbers in the silver borate glasses. In this way, E_0 was set to 25 516 eV on the absolute scale and S_0^2 to 0.8. The calculated amplitude and phase shift functions were used in the fit of the experimental EXAFS signal, back-Fourier filtered in the R-space range from 0.5 to 4.0 Å. The fit was performed in the k-space range 1.5–15.0 Å^{-1} using the four paths, which are sufficient to describe the c-Ag_2O EXAFS signal in the above-mentioned R-space range. These four paths correspond to the Ag-O_1-Ag, Ag-Ag_2-Ag, and Ag-O_3-Ag single-scattering signals from the first three nearest coordination shells around silver atom and to the Ag-O_1-Ag_2-Ag double-scattering signal. The calculated EXAFS signal for c-Ag_2O was in an excellent agreement with the experimental one (Fig. 1). The Ag-O_1 distance determined in
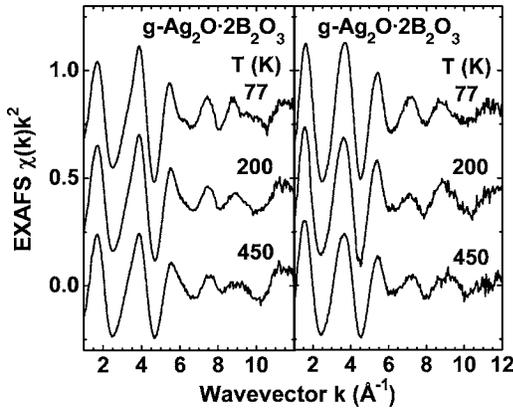
FIG. 2. Temperature dependence of experimental Ag K edge EXAFS signals $\chi(k)k^2$ in diborate g-$Ag_2O \cdot 2B_2O_3$ and tetraborate g-$Ag_2O \cdot 4B_2O_3$ glasses.

this way is 2.05±0.01 Å (the tabulated value is 2.044 Å),[34] the Ag-Ag$_2$ distance is 3.33±0.01 Å (the tabulated value is 3.338 Å), and the Ag-O$_3$ distance is 3.89±0.02 Å (the tabulated value is 3.914 Å). The fitted coordination numbers of the three nearest shells around Ag are 2.0±0.2, 11.5±0.6, and 6.5±0.8 while the crystallographic values are 2, 12, and 6. These results indicate a good accuracy of the theoretical amplitude and phase-shift functions for the Ag-O and Ag-Ag atom pairs in the k-space range of 1.5–15.0 Å^{-1}, which was used in the best-fit procedure for c-Ag_2O.

In the case of silver borate glasses, one needs the scattering amplitude and phase shift also for the Ag-B pair. These were found by performing FEFF8 calculations for a cluster representing a part of the silver orthoborate crystal structure.[35] The calculations were performed within the same approach as for c-Ag_2O, as described above.

C. EXAFS analysis in disordered systems

The EXAFS signal for an arbitrary radial distribution function $G(R)$, containing only one atomic species, is given, within the single-scattering spherical-wave approximation, by[36]

$$\chi(k) = S_0^2 \int_{R_{min}}^{R_{max}} \frac{G(R)}{kR^2} F(k,R) \sin[2kR + \Phi(k,R)] dR, \quad (2)$$

where the factor S_0^2 accounts for the amplitude damping caused by multielectron effects, R is the interatomic distance, $F(k,R)$ is the backscattering amplitude of the photoelectron from atoms located at the distance R from the photoabsorber, and $\Phi(k,R) = \psi(k,R) + 2\delta_l(k) - l\pi$ is the phase shift containing contributions from the photoabsorber $2\delta_l(k)$ and from the backscatterer $\psi(k,R)$. In the present notation, the amplitude $F(k,R)$ includes also the damping connected with the finite photoelectron lifetime. The amplitude and phase-shift functions $F(k,R)$ and $\Phi(k,R)$ were calculated for a fixed distance R in this work. Accounting for the R dependence of $F(k,R)$ and $\Phi(k,R)$ could be done in principle, and in some cases it can be important. One reason why we ignored it in our study is to avoid "technical" instabilities encountered by the FEFF8

code when calculating $F(k,R)$ and $\Phi(k,R)$ for too small or too large R. Another reason is that earlier XANES calculations showed that XAFS of borate is not very sensitive to the choice of the potential and, hence, to the $F(k,R)$ and $\Phi(k,R)$ functions (see end of Sec. III E).

When the extent of disorder (thermal and structural) is limited, the EXAFS function can be described by a sum of analytical functions, each one of which attributable to a different coordination shell and expressed through a cumulant expansion,[27,36]

$$\chi(k) = \sum_i S_0^2 \frac{N_i}{kC_{1i}^2} F_i(k,C_{1i})$$

$$\times \exp\left[-2C_{2i}^2 k^2 + \frac{2}{3}C_{4i}k^4 - \frac{4}{45}C_{6i}k^6\right]$$

$$\times \sin\left[2kC_{1i} - \frac{4}{3}C_{3i}k^3 + \frac{4}{15}C_{5i}k^5 + \Phi_i(k,C_{1i})\right],$$

$$(3)$$

where i labels the coordination shells, N_i is the coordination number, C_{1i} is the average value of an effective distribution,[27] C_{2i} is the mean-square relative displacement or Debye-Waller exponent (generally indicated as σ_i in Gaussian approximation), and C_{3i}, C_{4i}, C_{5i}, and C_{6i} are higher-order cumulants of the distribution of distances. This is the expression used by the EDAFIT code[33] to obtain the results presented in Sec. IV B. Neglect of higher-order cumulants C_{ji} $(j>2)$ leads to the multishell Gaussian approximation,[36] which is widely used in EXAFS analysis,[19] and where each Gaussian shell depends only on three structural parameters: N, C_1, and σ. It is worth noting that average interatomic distance is given by $\langle R_i \rangle \simeq C_{1i} + (2C_{2i}/C_{1i})(1 + C_{1i}/\lambda)$, where λ is the photoelectron mean free path. As we will see below, the standard approach based on Eq. (3) fails in the case of g-$Ag_2O \cdot nB_2O_3$. Therefore, one has to return to the original EXAFS formula and search for an arbitrarily shaped $G(R)$ by a direct inversion of Eq. (2). This technique is implemented in the EDARDF code, which relies on a hybrid regularization–least-squares-fitting algorithm[33] to search for a positive-defined and smooth $G(R)$ such that the best agreement between the simulated and experimental EXAFS is achieved.[37–39] There are also other procedures that one could rely on to determine $G(R)$, such as the regularization technique,[40] the splice method,[41] the Monte Carlo method,[42] and the reverse Monte Carlo technique.[43]

The advantage of relying on Eq. (2) instead of Eq. (3) is that no *a priori* assumptions about the shape of RDF are made. On the other hand, the RDF may now contain only one type of atoms, to guarantee the validity of the algorithm. This is not the case of the neighborhood of Ag ions in g-$Ag_2O \cdot nB_2O_3$: both O and B atoms are expected to be present. Because oxygen and boron atoms are close neighbors in the periodic table, their scattering amplitudes and phase shifts are quite similar. Therefore, one can expect that using scattering functions of only oxygens or of only borons will lead to a good estimate of the true RDF. As chemical considerations suggest that the nearest neighbors of Ag in
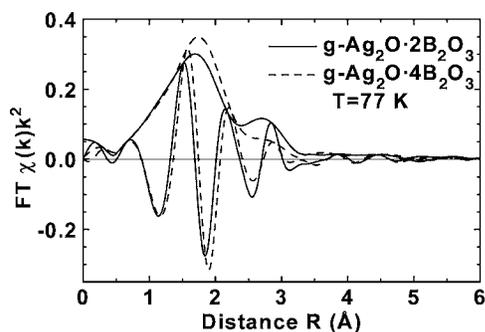
FIG. 3. Fourier transforms (FT) of experimental Ag K edge EXAFS signals in g-$Ag_2O \cdot 2B_2O_3$ (full lines) and g-$Ag_2O \cdot 4B_2O_3$ (dashed lines) at T=77 K.

g-$Ag_2O \cdot nB_2O_3$ should be oxygens, we relied on scattering functions of oxygens in our analysis. We checked that if the same analysis is performed with boron scattering functions instead, similar results about the shape of RDF and about its temperature dependence are obtained. Contributions from the Ag-Ag distance can be neglected, as it will follow from results of a standard analysis in Sec. IV A.

D. Estimation of the effect of multiple scattering

In this section, we comment on the use of the single-scattering approximation as represented by Eqs. (2) and (3). In general, the XAFS signal can be accurately described within the multiple-scattering (MS) formalism by an infinite series, which is usually truncated above a few first terms, known as single-scattering, double-scattering, and triple-scattering contributions.[20] Note that such series is not unique, and an alternative approach,[22] in which the XAFS signal is expanded in terms of the contributions from a number of irreducible n-atom distribution functions, also exists. The importance of different multiple-scattering signals in different regions of the k or R space was studied for years.[20,44,45] The MS signals were reliably detected in the case of near-linear atomic chains, e.g., in perovskite-type materials built up of octahedra, due to the so-called focusing effect.[44,46]

The amplitude of the MS contributions strongly depends on the geometry of the scattering paths as well as on the disorder. The positions of MS peaks in the Fourier transform (FT) are determined by the total half-path length. Therefore, significant MS scattering contributions are revealed in the FT through peaks at large distances, being located anyway beyond the first coordination shell peak.

We estimated the contribution of MS signals, due to the shortest scattering path lengths, in our borate glasses using the FEFF8 code.[21] Among different MS contributions, two signals with a particular geometry have the shortest total half-path length. If linear O-Ag-O chains were present in our glasses, considering the Ag-O distance about 2.3 Å, the presence of MS would result in a peak in FT at about 3.9 Å, having an amplitude of about 10% of the first shell peak (which is located at around 1.8 Å in Fig. 3). This MS peak would be generated by the double-scattering Ag-O′-O″-Ag and triple-scattering Ag-O′-Ag-O″-Ag signals (where Ag is the photoabsorber and O′ and O″ are two oxygens in oppo-

site directions).[44] If Ag atoms were coordinated tetrahedrally, the shortest MS signal would correspond to the triangular Ag-O′-O″-Ag double-scattering path, consisting of the photoabsorbing silver and two oxygens of the tetrahedron: its peak would be at about 3.5 Å in FT, having an amplitude of about 7% of the first shell peak.

Other MS signals would contribute at even larger distances because of longer scattering path lengths. Therefore, since no significant contributions above the level of noise are present in the FT of EXAFS signals of borate glasses at distances larger than 3.5 Å (Fig. 3), the MS signals can be ignored and, hence, there is no need to go beyond the single-scattering approximation in this particular case. Finally, let us note that even if MS contributions were present, they would not affect our EXAFS analysis, since that is limited to the first two peaks located below 3.2 Å in FTs of the EXAFS signals.

E. XANES calculations

The XANES spectrum of amorphous systems is usually calculated via a "single-configuration" approach, i.e., the signal is calculated just for a small unit surrounding the photoabsorbing atom.[47,48] This approach seems to be justified if the photoabsorbing atom is directly incorporated into a network (such as Si in silicates),[49,50] having thus a well-defined coordination polyhedron. However, the single-configuration approach fails in the case of Ag K edge XANES of g-$Ag_2O \cdot nB_2O_3$ because of the strong disorder around Ag ions.[29] A similar situation may arise wherever the photoabsorbing atom is not a glass network former but just a network modifier.

For such cases, we propose to use a multiconfiguration approach.[29] It is based on evaluating the XANES of the system as an average of individual signals calculated for a large number (hundreds) of geometric configurations, which are randomly generated subject to certain constraints on atomic positions. These constraints then represent structural information that can be obtained for the system. It was demonstrated that, although this procedure cannot determine the RDF with the same accuracy as EXAFS, it can still be useful, particularly because of its sensitivity to chemical types of neighboring atoms.[29]

In the present work, XANES spectra of g-$Ag_2O \cdot nB_2O_3$ are calculated via a multiconfiguration approach, relying on the RDF obtained from EXAFS. Spectra of individual geometric configurations are calculated in the real space by a full-multiple-scattering (FMS) technique.[51] We used the same scattering potential for all the clusters—in particular, a non-self-consistent muffin-tin potential constructed via a Mattheiss prescription for a silver orthoborate crystal[35] (c-$Ag_2O \cdot 3B_2O_3$). We checked that this particular choice of the potential is not crucial, which is not surprising: one can expect that errors caused by the inaccuracy of the potential will be significantly smaller than errors caused by the inaccuracies of various structural models. More details about XANES calculations can be found in our earlier paper.[29] It is worth noting that if the XANES analysis is not particularly sensitive to the choice of the scattering potential, the same will be

also true for EXAFS. Thus, the use of the orthoborate structure for generating EXAFS scattering amplitude and phase-shift functions for the Ag-B pair (see Sec. III B) is not really a restriction.

IV. RESULTS

A. EXAFS data analysis

Weighted experimental Ag K edge EXAFS signals $\chi(k)k^2$ of silver borate glasses are shown in Fig. 2. Low noise is maintained even at relatively large k values for both chemical compositions and for all temperatures. The signals from diborate and tetraborate glasses are similar but still different and exhibit a small but noticeable temperature dependence. This demonstrates the quality of experimental data and the stability of our procedure for extracting EXAFS oscillations. A notable feature is the absence of any strong high-frequency contribution from distant coordination shells; apparently, they are smeared out by a strong static disorder. At the same time, the EXAFS signals show evidence of the interference between several oscillating contributions. This is clearly visible in Fig. 3, where we present the FTs of the experimental EXAFS signals. The FTs were calculated using a Kaiser-Bessel window function in the k space spanning from 2 to 9 Å^{-1}. Note that the positions of peaks in FTs differ from the true crystallographic values because of the scattering amplitude and phase-shift contributions to the EXAFS signals. All FTs have a double peak shape, with no significant signal above ~ 3.5 Å. The difference between the diborate and the tetraborate signals is clearly seen. The absence of long-range order in $g\text{Ag}_2\text{O} \cdot n\text{B}_2\text{O}_3$ allows us to analyze the experimental EXAFS signals without employing the Fourier filtering procedure. In that way, the distortions, which are often introduced due to the finite k-space interval, can be avoided.

The results of the EXAFS analysis reported below were obtained by best fitting the signal in the k space in the interval from 2 to 9 Å^{-1}. Several other intervals were also used (2−7 Å^{-1}, 3−9 Å^{-1}, and 1−10 Å^{-1}) to verify the stability of our solution. The results do not differ substantially between these intervals. However, the fitting error increases slightly for the largest interval, mainly due to the artifact in the experimental data at about 10 Å^{-1}. It is caused by some noise present in the experimental signal, which hinders the correct determination of the atomiclike signal $\mu_0(E)$ at high energies (see Sec. III A). An additional—although small—contribution to the increase of the fitting error for the 1−10 Å^{-1} interval is the lower accuracy of the backscattering amplitude and phase-shift functions, calculated by FEFF8 code,[21] at low k values. The narrowing of the fitting interval to 2−7 Å^{-1} or 3−9 Å^{-1} gives essentially the same result as for the 2−9 Å^{-1} interval, with a slightly more broadened RDF owing to the expected decrease of spatial resolution.[37] Hence, although it is not always possible, in general, to extend the low-k end of the fitting interval down to $k=2$ Å^{-1}, our analysis suggests that it is reasonable for the systems we study.

Finally, one should point out that the analysis of the EXAFS signal in the low-k region is always beneficial for precise estimation of coordination numbers, when reliable amplitude and phase-shift functions are available, and is crucial in the case of large disorder, which results in rapidly damped EXAFS signal.

B. Cumulant expansion and multishell Gaussian model

Early EXAFS studies of silver borate glasses at the Ag K and L_3 edges, performed within the single-shell Gaussian approximation, suggested that Ag ions are surrounded by only two oxygens, located at the distance of 2.27–2.30 Å.[12–14] A simple but accurate analysis of the present new data within the single-shell formalism, by Fourier filtering of the first-shell contribution and including higher-order cumulants, led again to similar results—including the very low number of oxygen atoms contributing to the first main peak in the FT. The coordination numbers obtained thereby are significantly smaller than those found by x-ray and neutron scattering studies.[5,9,11] This disagreement has probably to be attributed to the inadequacy of a single-shell treatment of EXAFS data (in spite of including high order cumulants) in the case of RDFs broadened by the presence of strongly asymmetric or complex shapes. Actually, interference effects in very broad RDF can significantly reduce the amplitude of EXAFS oscillations and the corresponding height of FT peaks, as it can be seen by comparing the signals in Figs. 2 and 3 for glasses and in Fig. 1 for *c*-Ag$_2$O; thus, no reliable information on coordination numbers can be obtained from a simple visual comparison with the FT of a reference compound. Moreover, non-negligible distortions of the filtered EXAFS signals can be introduced when attempting to separate overlapping peaks in FT. Therefore, we did not use Fourier filtering in further procedures, evaluating all the possible contributions to EXAFS together.

As a next step, we analyzed EXAFS using a multishell model, attempting to best-fit the complete experimental EXAFS signal using up to three different Gaussian-type shells. Such a model involves up to nine parameters, which is below the upper limit of 14 predicted by the Nyquist criterion.[52,53] Each Gaussian shell corresponds to a group of either oxygens or borons.

Typical results of the best fit using a two-Gaussian model are shown in Fig. 4. A careful analysis of the results obtained from the best-fitting procedures indicates that the two-shell models are inadequate to reproduce the experiment with a sufficient accuracy, especially for diborate glass. They suggest, in any case, the presence of many more atoms (about eight to nine) distributed in a very disordered situation, as documented by a very high Debye-Waller factor (mainly for the second shell) and the superposition of Gaussian distributions. The insertion of asymmetry or other broadening terms did not modify significantly the results. Of course, the three-shell model provided much better agreement between experimental and calculated signals. Unfortunately, the quantitative results for the three-shell model were unstable—unphysical variations of N, R, and σ occur if the temperature or the Ag$_2$O content is changed. A further model including silver atoms was also considered; however, the addition of the Ag contribution did not result in a significant improvement of the quantitative analysis.
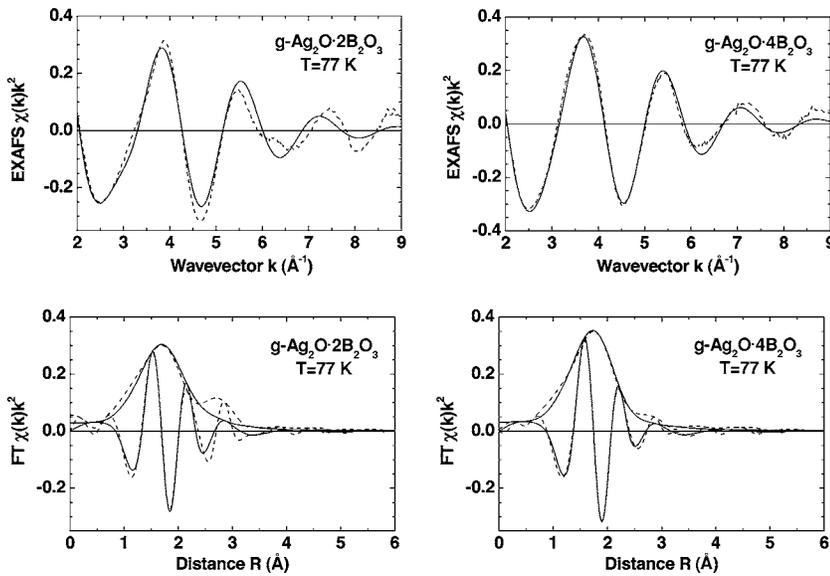
FIG. 4. Result of best fitting of the Ag K edge EXAFS of g-$Ag_2O \cdot 2B_2O_3$ and g-$Ag_2O \cdot 4B_2O_3$ using a two-Gaussian RDF containing only oxygen atoms. Experimental signal is shown by dashed lines, theoretical signal by full lines.

We conclude, therefore, that neither the single-shell cumulant expansion nor the analysis based on a multishell Gaussian *ansatz* for RDF can be applied satisfactorily to g-$Ag_2O \cdot nB_2O_3$.

C. Model independent RDF reconstruction

We turn now to a model-independent reconstruction of RDF via the EDARDF code, as outlined in Sec. III C. The RDFs $G(R)$ were defined on a grid from 0.8 to 3.8 Å with a grid step of 0.03 Å. The comparison between best-fitted signals and experiments for the case of $T = 77$ K is presented in Fig. 5. An excellent agreement can be observed in both the k and R spaces. The same level of agreement between calculated and experimental EXAFS signals was achieved for all temperatures. The reconstructed RDFs around Ag in g-$Ag_2O \cdot 2B_2O_3$ and g-$Ag_2O \cdot 4B_2O_3$ for three selected temperatures are presented in Fig. 6. These RDFs are broad, extending from $\sim$1.9 Å to $\sim$3.3 Å, and have a complex

shape due to at least two strongly overlapping contributions.

The first contribution has its maximum at 2.31 Å in the diborate and at 2.39 Å in the tetraborate glasses. This peak is sharper in g-$Ag_2O \cdot 4B_2O_3$ than in g-$Ag_2O \cdot 2B_2O_3$. In both glasses, the influence of thermal disorder on the nearest neighborhood of Ag is monitored by the progressive reduction of the intensity of the first contribution to the $G(R)$ when temperature increases, while no significant changes can be detected in the peak position.

The second contribution to the RDF, located between 2.5 and $3.2 – 3.5$ Å, has a smaller amplitude and is much broader than the first contribution. Its shape is slightly different in the two glasses, being $\sim$0.2 Å wider in the tetraborate glass. Because of its large width, this second contribution corresponds to a strongly damped EXAFS signal in k space, with an amplitude that quickly decays with increasing k. This fact, together with the above-mentioned difficulty in distinguishing between oxygen and boron atoms, greatly complicates an accurate determination of the RDF in this range of distances,
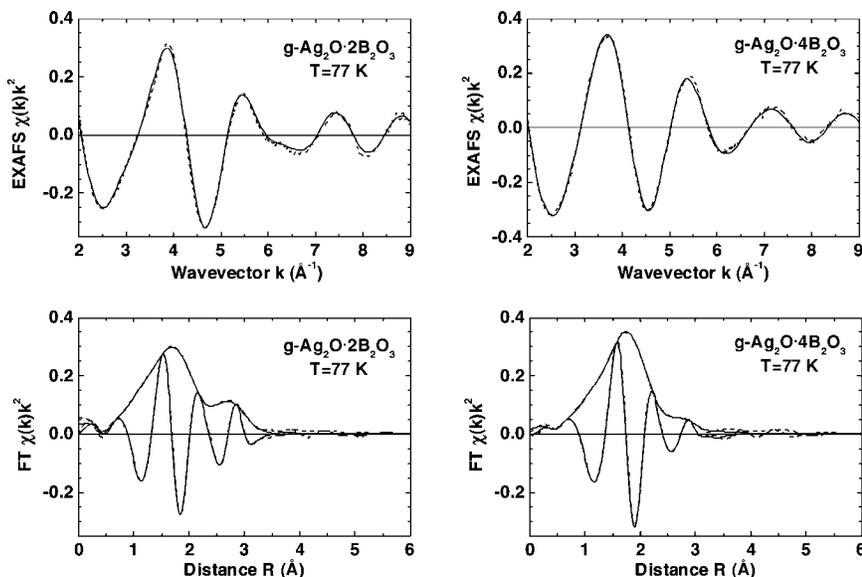
FIG. 5. Result of best fitting of the Ag K edge EXAFS of g-$Ag_2O \cdot 2B_2O_3$ and g-$Ag_2O \cdot 4B_2O_3$ using a model-independent reconstruction of RDF. Experimental signal is shown by dashed lines, theoretical signal by full lines (both lines are often indistinguishable from one another).
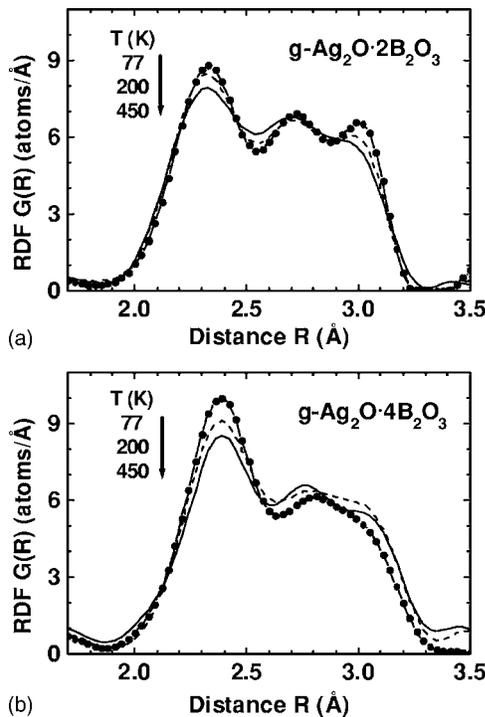
FIG. 6. Temperature dependence of the radial distribution functions $G(R)$ in g-$Ag_2O \cdot 2B_2O_3$ and g-$Ag_2O \cdot 4B_2O_3$, as determined from best fitting of the Ag K edge EXAFS.

as well as the interpretation of its temperature dependence. Atoms farther from Ag than ~ 3.5 Å apparently do not contribute to the EXAFS signal at all, presumably due to a strong static disorder in their positions with respect to Ag.

One should note that coordination numbers N cannot be attributed unambiguously to the two contributions singled out by EXAFS. However, a rough estimate can be made by approximating the true RDF by two Gaussians, as it is done in Fig. 7. From the area of these Gaussians one can find that there are about four atoms in each RDF component.

In summary, the analysis of EXAFS data confirms the presence of a strong static disorder around Ag ions that cannot be described in terms of a simple Gaussian broadening of multiple shells. On the other hand, one can find a more gen-
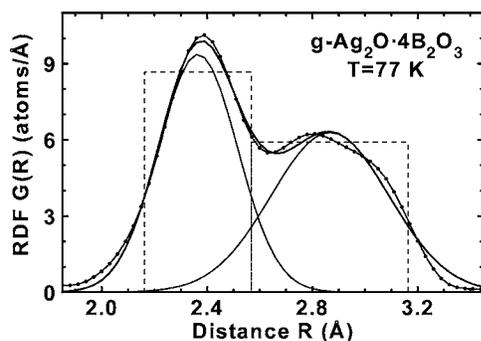
FIG. 7. $G(R)$ of g-$Ag_2O \cdot 4B_2O_3$ at $T=77$ K determined by best fitting the EXAFS signal (full line with dots) and its approximation by a double Gaussian function (full lines without dots) and by a semiuniform distribution (dashed lines).

eral shape for the RDF around Ag by a model-independent analysis of EXAFS. This RDF contains the contribution of about four atoms in the range 2–2.5 Å, and at least four other atoms in the range 2.5–3.5 Å. The first contribution shows an increasing thermal disorder if the temperature is increased. The second contribution to RDF is more complicated because it involves atoms distributed in a wide range, with significant differences between diborate and tetraborate glasses. As a whole, these findings are consistent with the local geometry around Ag atoms in silver borate crystals.[35,54,55]

D. Analysis of XANES

When performing a multiconfiguration analysis of XANES, we assume that the Ag-related RDF is already known from EXAFS (Sec. IV C). Hence, the individual geometric configurations have to be generated in such a way that the average distribution of the Ag–X distances $(X=O,B)$ coincides with this RDF. To simplify the matters technically, we focused on g-$Ag_2O \cdot 4B_2O_3$ and approximated its EXAFS-derived RDF (Fig. 6) by a superposition of two Gaussians, as shown in Fig. 7. We will see later that this does not restrict the validity of our conclusions. Similarly, as argued in our earlier paper,[29] atoms that are more distant than those described by the EXAFS-derived RDF can be ignored because their contributions essentially cancel in the presence of disorder.

We generated several sets of geometric configurations ("structural models"), differing one from another by the average number of boron atoms K_B. The boron atoms were preferentially placed into the more distant of the two approximating Gaussians; only if $K_B \geq 4$, some borons were put into the first shell as well. For each set of configurations we obtained theoretical K edge XANES by calculating the spectrum for each individual configuration and averaging them afterward. In our case, each set contained 200 different configurations.

XANES calculated for these structural models is compared to the experiment for g-$Ag_2O \cdot 4B_2O_3$ in Fig. 8. The experimental XANES has two main peaks, one at 20 eV and one at 60–65 eV above the edge (the E_0 used in our EXAFS analysis corresponds to 12 eV in the scale of Fig. 8). The first peak is more pronounced, whereas the second one is broad and corresponds to the maximum at ~ 3.7 Å^{-1} in Fig. 9. The XANES signals show a clear dependence on the average number (K_B) of boron atoms in the cluster. For small K_B, the first peak at about 20 eV has a much smaller amplitude than in the experiment. By increasing the number of borons, the XANES signal becomes closer to the experimental one at about $K_B=4$. Further increase of the boron content results in a decrease of the first peak amplitude and an appearance of a spurious pre-edge peak at 8 eV.

To compare the calculated and experimental XANES signals in a more quantitative way, one can use the R^2 factor, defined as
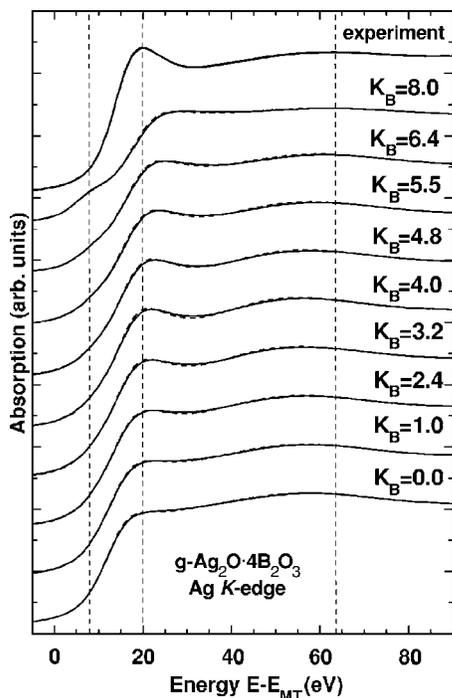
FIG. 8. Theoretical Ag K edge XANES for g-$Ag_2O \cdot 4B_2O_3$. The spectra were calculated for atomic configurations consistent with double Gaussian (full lines) and semiuniform (dashed lines) distribution functions, as shown in Fig. 7. Each structural model is characterized by the average number of borons K_B; remaining $(8-K_B)$ atoms are oxygens. Vertical lines are guides for the eye. Note that E_0 of Fig. 2 corresponds to 12 eV in this graph.

$$R^2 = 100 \frac{\int dE[Y_{the}(E) - Y_{exp}(E)]^2}{\int dE[Y_{exp}(E)]^2},$$

where Y_{the} and Y_{exp} are the theoretical and experimental spectral intensities, respectively. We evaluated this R^2 factor for each of the theoretical curves shown in Fig. 8 in the energy range from −5 eV to 90 eV. The results are summarized in Table I. One can see that the models containing 4.0–5.5 borons are the most plausible ones, based on the R^2-factor criterion. A mechanical comparing of R^2 factors should be, nevertheless, used with caution in XANES. This criterion is, namely, tailored for comparing oscillating EXAFS-like functions, which are obtained after the background has been subtracted. In XANES, on the other hand, the absorption edge is an essential part of the spectrum and cannot be removed in an unambiguous way. A less rigorous but more comprehensive visual inspection of the spectra is thus more appropriate in this case, because it can account for trends and features whose quantification cannot be automated in a simple way.[29]

The main outcome of this section, namely, that the nearest Ag neighborhood contains around $K_B=4-5$ borons, does not depend on the particular details of the RDF used as a constraint for generating individual geometric configurations. To verify this, we calculated XANES also for a semiuniform

TABLE I. The R^2 factors characterizing the difference between theoretical XANES spectra of g-$Ag_2O \cdot 4B_2O_3$, shown in Fig. 8, and the experiment.

Number of borons	R^2
0.0	0.2999
1.0	0.2708
2.4	0.2389
3.2	0.2112
4.0	0.1860
4.8	0.1849
5.5	0.1867
6.4	0.2084
8.0	0.3276

RDF that is piecewise constant within two nonoverlapping intervals ranging from 2.17 to 2.57 Å and from 2.57 to 3.17 Å and its height is such that the number of atoms in each of these two intervals is four. This RDF is depicted by dashed lines in Fig. 7. The resulting XANES curves are shown in Fig. 8 with dashed lines. One can see that the difference between spectra calculated for the double Gaussian and for the semiuniform RDF is very small, suggesting that XANES is much less sensitive to the shape of the RDF than EXAFS, at least in this particular case. This is also the reason why it is not really important whether we generate the individual configurations so that they conform the true RDF or its double Gaussian approximation.

One can see from Fig. 8 and Table I that XANES spectra for $K_B=4.0-5.5$ yield all approximately the same agreement
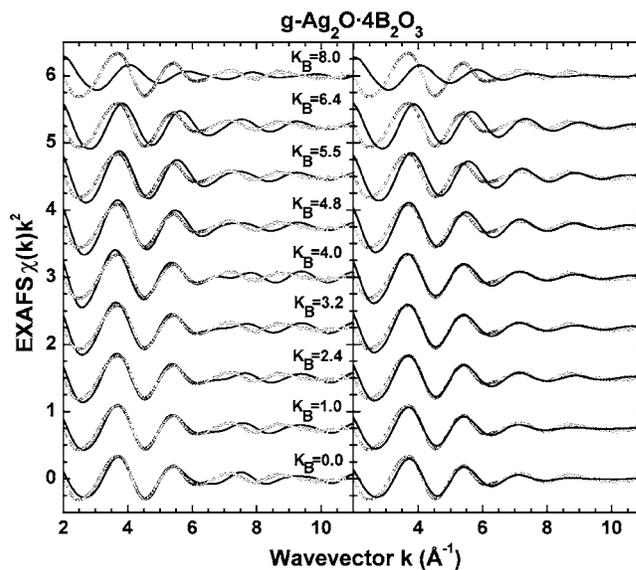
FIG. 9. Comparison between the experimental Ag K edge EXAFS of g-$Ag_2O \cdot 4B_2O_3$, measured at $T=77$ K, with the theoretical EXAFS calculated for models conforming the semiuniform radial distribution (left panel) and conforming the double Gaussian distribution of Fig. 7 (right panel). The experimental signal is shown by open circles, the calculated signals are shown by full lines. The number of borons K_B is the same as in Fig. 8.

with experiment. Therefore one can view this interval as the accuracy with which K_B can be determined from XANES. This also means that this estimate of K_B is valid not only for g-Ag$_2$O·4B$_2$O$_3$ but for g-Ag$_2$O·2B$_2$O$_3$ as well. Performing the same kind of analysis for g-Ag$_2$O·2B$_2$O$_3$ instead of for g-Ag$_2$O·4B$_2$O$_3$ would mean, namely, to repeat the analysis of this section with our RDF shifted by about 0.1 Å to the shorter distances (see Fig. 6). However, that was, in fact, already done by Šipr *et al.*[29] who arrived at a similar conclusion concerning K_B by relying on a semiuniform RDF distribution with the first four atoms between 2.0 and 2.4 Å and the other four atoms between 2.5 and 3.0 Å. Given the small sensitivity of XANES to the details of RDF and the above-mentioned accuracy with which K_B can be determined, it is obvious that any reasonable approximation of any of the RDFs shown in Fig. 6 would lead to the same conclusion about K_B.

E. Configurationally averaged EXAFS calculation

By employing the direct inversion of EXAFS formula as described in Sec. IV A, one cannot discriminate between O and B atoms. The multiconfiguration approach makes it possible to check the sensitivity of EXAFS to chemical types of Ag neighbors. For that purpose, we calculated the EXAFS signal by averaging it over the same set of geometric configurations as used for XANES simulations. As in Sec. IV D, to simplify matters technically, we will consider only the case of tetraborate glass, whose RDF at 77 K has a shape that is close enough to a sum of two Gaussian functions (Fig. 7). This is, in fact, the most simple situation among all the analyzed spectra, for which the corresponding RDF cannot be described by a sum of two Gaussians (cf. Fig. 6). The present approach can be, however, extended to an arbitrary RDF in a straightforward way.

It is worth noting that, although the double-Gaussian RDF model investigated in this section and the two-shell Gaussian model discussed in Sec. IV B have similar RDFs as concerns their shapes, they differ in the chemical composition: while only oxygen atoms were contributing to the two-shell Gaussian model, here a part of oxygen atoms is substituted by the same number K_B of *randomly* placed borons. Therefore, the present model is more plausible from the chemical point of view. However, it is necessary to remember that no fitting was attempted in this section, therefore one should not expect to get a perfect agreement between configurationally averaged EXAFS signal and experiment.

Because the double Gaussian and semiuniform distributions give very similar results in the XANES region (Fig. 8), we checked here also to what extent the difference between both distributions is reflected through the EXAFS. The results of configurationally averaged EXAFS calculations are summarized in Fig. 9 (the left panel shows the spectra calculated for the semiuniform RDF and the right panel for the double-Gaussian RDF). It is interesting—though not surprising—that EXAFS is indeed more sensitive to the shape of RDF than XANES: in general, the double-Gaussian RDF is more able to reproduce the experimental spectrum of tetraborate glass at T=77 K. In fact, while at low k (k

<6 Å^{-1}) both distributions work quite fine for small and intermediate boron content (K_B<6), for large k, the results for a semiuniform RDF deviate considerably from the experiment.

As concerns the effect of varying the boron content, it can be seen that in the absence of boron atoms (K_B=0), the EXAFS oscillations generated by the double-Gaussian RDF are more damped at high k values than observed experimentally (note that a similar deficiency occurs also for a proper two-shell Gaussian model, as presented in the upper right graph of Fig. 4). For $K_B \simeq 4$, the agreement is the best. For a large number of borons (K_B>4), the theoretical EXAFS has different frequency and is progressively damped, already at low k values. So the multiconfiguration analysis of EXAFS confirms the conclusion of Sec. IV D about the chemical composition of silver ions neighborhood.

Finally, one should point out that the agreement between theory and experiment for any of the models presented in Fig. 9 is worse than for the model investigated in Fig. 5. This is connected with the fact that the model investigated in the current section conforms only the double-Gaussian approximation to the non-Gaussian distribution (cf. Fig. 7).

V. DISCUSSION

The RDFs shown in Fig. 6 represent *average* radial distributions. That does not necessarily imply that a majority of Ag ions will have this RDF around them. Rather, the glasses will contain several inequivalent Ag sites, with differing RDFs. These site-dependent RDFs will have to be, nevertheless, such that the average of RDFs around all Ag ions will be that shown in Fig. 6. Our results thus can be viewed as a constraint that more complete structural models of g-Ag$_2$O·nB$_2$O$_3$ will have to obey. For example, far infrared absorption spectroscopy presents compelling evidence[56] that—as concerns their vibrational properties—there are two inequivalent Ag sites in g-Ag$_2$O·nB$_2$O$_3$. It follows from our analysis that the difference between both Ag sites will not consist in having two very different Ag-O distances (because, in such a case, a double-peak structure would have to appear in Fig. 6); probably, the sites will differ in their second-nearest-neighbor distances and/or coordination numbers.

Separate Ag-O and Ag-B contributions to RDF around Ag ions were obtained in the past by a reverse Monte Carlo (RMC) analysis of neutron and x-ray scattering data for g-Ag$_2$O·2B$_2$O$_3$ (Ref. 9) and of neutron scattering data for g-Ag$_2$O·4B$_2$O$_3$.[11] Our results generally agree with results of RMC analysis of Swenson *et al.*[9,11] In both cases, the RDF around Ag is characterized by a well-defined peak containing mostly O atoms, followed by a less intensive but broader peak containing mostly borons. The first Ag-O peak in the RDF of Swenson *et al.*[9,11] is, however, much sharper and more intensive than the corresponding first RDF peak in our Fig. 6. Also, the Ag-O and Ag-B contributions are clearly separated in the simulations of Swenson *et al.*, while in our case both species are intermixed: the O-dominated region continuously merges into the B-dominated region. As concerns the distances, the analysis of Swenson *et al.*[9,11] puts the

maximum intensity of the first Ag-O peak at 2.4 Å for both g-Ag$_2$O·2B$_2$O$_3$ and g-Ag$_2$O·4B$_2$O$_3$, while in our case the mean Ag-O distance increases with boron content—from 2.31 Å for g-Ag$_2$O·2B$_2$O$_3$ to 2.39 Å for g-Ag$_2$O·4B$_2$O$_3$. Our analysis, which makes no initial assumptions about the shape of RDF, can also be used for an *a posteriori* check of the limits imposed on the interatomic distances during the RMC analysis of scattering data. Swenson *et al.*[9,11] assumed that the Ag-O distance has to be larger than 2.1 Å and the Ag-B distance has to be larger than 2.6 Å. Our analysis yields appreciable Ag-O contribution for distance as small as 2.0 Å and Ag-B contribution for distance as small as 2.4 Å. It seems, therefore, that the limits imposed by Swenson *et al.*[9,11] were too stringent—especially for the Ag-B case (that could be inferred also from the unusually sharp onset of the Ag-B distribution function in Ref. 9).

In order to exploit the full potential of XAFS, one needs to analyze both EXAFS and XANES. Namely, each of the techniques is sensitive to a particular aspect of the local geometry while being significantly less sensitive to the other aspect: EXAFS is quite sensitive to details of the RDF and not very sensitive to the chemical type of Ag neighbors, XANES is not very sensitive to the details of RDF but is quite sensitive to the content of boron atoms K_B. For example, it would be not possible to estimate K_B solely from multiconfiguration EXAFS analysis as displayed in Fig. 9 because the same effect on the calculated EXAFS curves that is caused by changing K_B could be imitated by a slight change of the RDF. On the other hand, because XANES is not very sensitive to the details of the RDF, one can be quite certain that the changes of the calculated XANES spectrum connected with varying K_B would be the same no matter what (no-nonsense) RDF is employed. In that way, weak points of each of the two techniques actually turn into advantages if they are applied jointly.

Another important point to note is that it was possible to extract reliable structural information from either EXAFS or XANES only after one acknowledged the existence of a strong static disorder around Ag and resorted to a search for a site-averaged RDF. It would not be possible to obtain stable results if one insisted on splitting the Ag neighborhood into well-defined coordination shells and tried to find R, N, and σ associated with them. Our approach can be thus viewed as a trade-off between specificity and robustness. We suggest that this kind of approach ought to be preferred whenever dealing with systems with a strong short-range disorder.

VI. SUMMARY AND CONCLUSIONS

The local environment around Ag ions in silver borate glasses g-Ag$_2$O·nB$_2$O$_3$ (n=2,4) has been studied at the Ag K edge by x-ray absorption spectroscopy in the temperature range from 77 to 450 K. Because of the strong disorder around Ag ions in these glasses, methods of EXAFS analysis based on Fourier filtering and cumulant expansion do not provide reliable results. A method based on a direct inversion of the EXAFS formula, which does not depend on any *a priori* assumptions about the shape of the RDF, was therefore applied in order to reconstruct the RDF around Ag ions via best fitting of experimental EXAFS signal. However, this technique does not make it possible to specify the chemical types of atoms which surround Ag ions, because the proximity of boron and oxygen in the periodic table does not allow one to separate unambiguously their contributions to EXAFS (and, consequently, to RDF). To overcome this problem, configurationally averaged simulations of the Ag K edge XANES were performed, relying on the RDF obtained from EXAFS analysis. The complementarity of EXAFS and XANES techniques thus allowed us to determine a more complete structural model than would be possible by relying solely on either EXAFS or XANES alone.

The local neighborhood of Ag ions is strongly disordered, with appreciable non-Gaussian contribution to the RDF. Quantitatively, silver is surrounded by about four atoms, mainly oxygens, with their distribution peaked around 2.31 Å in diborate and around 2.39 Å in tetraborate glasses. The second RDF peak corresponds mainly to borons and is very broad, extending from about 2.5 Å to 3.2–3.4 Å, with its center around 2.9 Å. Both peaks strongly overlap. Although static disorder dominates in the neighborhood of Ag ions, the first RDF peak still exhibits also some temperature dependence.

The structural parameters we obtained are in a good agreement with the results of x-ray and neutron scattering studies.[9,11] Strong overlap between oxygen and boron subshells explains why underestimated values of the Ag–O distance and coordination number have been found in previous EXAFS studies.[12–14]

*Electronic address: a.kuzmin@cfi.lu.lv; URL: http//www.cfi.lu.lv

[1] T. Minami, J. Non-Cryst. Solids **73**, 273 (1985).

[2] G. Calas, L. Cormier, L. Galoisy, and P. Jollivet, C. R. Chim. **5**, 831 (2002).

[3] G. Licheri, A. Musinu, G. Paschina, G. Piccaluga, and G. Pinna, J. Chem. Phys. **85**, 500 (1986).

[4] L. Börjesson, L. M. Torell, and W. S. Howells, Philos. Mag. B **59**, 105 (1989).

[5] J. Swenson, L. Börjesson, and W. S. Howells, Phys. Rev. B **52**, 9310 (1995).

[6] H. Ushida, Y. Iwadate, T. Hattori, S. Nishiyama, K. Fukushima, M. Misawa, and T. Fukunaga, J. Alloys Compd. **327**, 121 (2001).

[7] L. Červinka, F. Rocca, P. Fornasini, and G. Dalba, J. Non-Cryst. Solids **150**, 140 (1992).

[8] L. Červinka and F. Rocca, J. Non-Cryst. Solids **192-193**, 125 (1995).

[9] J. Swenson, L. Börjesson, R. L. McGreevy, and W. S. Howells, Phys. Rev. B **55**, 11236 (1997).

[10] L. Červinka, J. Bergerová, A. Dalmaso, and F. Rocca, J. Non-Cryst. Solids **232-234**, 627 (1998).

[11] J. Swenson, L. Börjesson, and W. S. Howells, J. Phys.: Condens. Matter **11**, 9275 (1999).

[12] G. Dalba, P. Fornasini, and F. Rocca, J. Phys. (Paris), Colloq. **46**, C8-101 (1985).

[13] G. Dalba, P. Fornasini, F. Rocca, E. Bernieri, E. Burattini, and S. Mobilio, J. Non-Cryst. Solids **91**, 153 (1987).

[14] G. Dalba, P. Fornasini, and F. Rocca, J. Non-Cryst. Solids **123**, 310 (1990).

[15] G. Dalba, P. Fornasini, A. Fontana, F. Rocca, and E. Burattini, Solid State Ionics **28-30**, 713 (1988).

[16] F. Rocca, G. Dalba, P. Fornasini, and A. Tomasi, Solid State Ionics **53-56**, 1253 (1992).

[17] G. Dalba, P. Fornasini, F. Rocca, and F. Monti, J. Non-Cryst. Solids **293-295**, 93 (2001).

[18] G. Dalba, P. Fornasini, R. Grisenti, S. a Beccara, N. Daldosso, A. Sanson, F. Rocca, F. Monti, and A. Kuzmin, Phys. Chem. Glasses **44**, 75 (2003).

[19] See papers published in *Proc. 12th Int. Conf. on X-ray Absorption Fine Structure, Malmö, 2003*, edited by D. Arvanitis, Phys. Scr. **T115** (2005).

[20] J. J. Rehr and R. C. Albers, Rev. Mod. Phys. **72**, 621 (2000).

[21] A. L. Ankudinov, B. Ravel, J. J. Rehr, and S. D. Conradson, Phys. Rev. B **58**, 7565 (1998).

[22] A. Filipponi, A. Di Cicco, and C. R. Natoli, Phys. Rev. B **52**, 15122 (1995).

[23] N. Binsted and S. S. Hasnain, J. Synchrotron Radiat. **3**, 185 (1996).

[24] Y. Joly, Phys. Rev. B **63**, 125120 (2001).

[25] M. Benfatto, S. Della Longa, and C. R. Natoli, J. Synchrotron Radiat. **10**, 51 (2003).

[26] G. Bunker, Nucl. Instrum. Methods Phys. Res. **207**, 437 (1983).

[27] P. Fornasini, F. Monti, and A. Sanson, J. Synchrotron Radiat. **4**, 243 (1997).

[28] P. Fornasini, S. a Beccara, G. Dalba, R. Grisenti, A. Sanson, M. Vaccari, and F. Rocca, Phys. Rev. B **70**, 174301 (2004).

[29] O. Šipr, G. Dalba, and F. Rocca, Phys. Rev. B **69**, 134201 (2004).

[30] G. Dalba, P. Fornasini, A. Kuzmin, F. Monti, A. Sanson, O. Šipr, and F. Rocca, Phys. Scr. **T115**, 149 (2005).

[31] A. Magistris, G. Chiodelli, and A. Schiraldi, Electrochim. Acta **24**, 203 (1979).

[32] A. Kuzmin, Physica B **208/209**, 175 (1995).

[33] A. Kuzmin, *EDA: EXAFS Data Analysis Software Package User's Manual*, Institute of Solid State Physics, Riga (2001); available at http://www.dragon.lv/eda

[34] R. W. G. Wyckoff, Am. J. Sci. **3**, 184 (1922).

[35] M. Jansen and W. Scheld, Z. Anorg. Allg. Chem. **477**, 85 (1981).

[36] B. K. Teo, *EXAFS: Basic Principles and Data Analysis* (Springer-Verlag, Berlin, 1986).

[37] A. Kuzmin, J. Phys. IV **7**, C2-213 (1997).

[38] A. Kuzmin and J. Purans, J. Phys.: Condens. Matter **12**, 1959 (2000).

[39] A. Kuzmin, J. Purans, G. Dalba, P. Fornasini, and F. Rocca, J. Phys.: Condens. Matter **8**, 9083 (1996).

[40] Yu. A. Babanov, V. V. Vasin, A. L. Ageev, and N. V. Ershov, Phys. Status Solidi B **105**, 747 (1981).

[41] E. A. Stern, Y. Ma, O. Hanske-Petitpierre, and C. E. Bouldin, Phys. Rev. B **46**, 687 (1992).

[42] P. Kizler, in *Proc. 6th Inter. Conf. on X-ray Absorption Fine Structure, York, August 5–11, 1990*, edited by S. S. Hasnain (Ellis Horwood, Singapore, 1991), p. 78.

[43] R. L. McGreevy, J. Phys.: Condens. Matter **13**, R877 (2001).

[44] A. Kuzmin, J. Purans, M. Benfatto, and C. R. Natoli, Phys. Rev. B **47**, 2480 (1993).

[45] A. Kuzmin and R. Grisenti, Philos. Mag. B **70**, 1161 (1994).

[46] A. Kuzmin and J. Purans, J. Phys.: Condens. Matter **5**, 9423 (1993).

[47] O. Yanagisawa, T. Fujikawa, and S. Naoe, Jpn. J. Appl. Phys., Part 1 **37**, 230 (1998).

[48] A. N. Mansour, A. Marcelli, G. Cibin, G. Yalovega, T. Sevastyanova, and A. V. Soldatov, Phys. Rev. B **65**, 134207 (2002).

[49] F. Farges, G. E. Brown, Jr., A. Navrotsky, H. Gan, and J. J. Rehr, Geochim. Cosmochim. Acta **60**, 3039 (1996).

[50] Z. Wu, C. Romano, A. Marcelli, A. Mottana, G. Cibin, G. Della Ventura, G. Giuli, P. Courtial, and D. B. Dingwell, Phys. Rev. B **60**, 9216 (1999).

[51] D. D. Vvedensky, in *Unoccupied Electron States*, edited by J. C. Fuggle and J. E. Inglesfield (Springer-Verlag, Berlin, 1992), p. 139; C. R. Natoli, M. Benfatto, S. Della Longa, and K. Hatada, J. Synchrotron Radiat. **10**, 26 (2003).

[52] E. O. Brigham, *The Fast Fourier Transform* (Prentice-Hall, Englewood Cliffs, NJ, 1974).

[53] E. A. Stern, Phys. Rev. B **48**, 9825 (1993).

[54] G. Brachtel and M. Jansen, Z. Anorg. Allg. Chem. **478**, 13 (1981).

[55] J. Krogh-Moe, Acta Crystallogr. **18**, 77 (1965).

[56] J. A. Kapoutsis, E. I. Kamitsos, and G. D. Chryssikos, in *Borate Glasses, Crystals and Melts*, edited by A. C. Wright, S. A. Feller, and A. C. Hannon (Society of Glass Technology, Sheffield, 1992), pp. 303–312.